Supporting Information

Rational Design of 3D N-doped Carbon Nanosheet Framework Encapsulated Ultrafine ZnO Nanocrystals as Superior Performance Anode Materials in Lithium Ion Batteries

Jianding Li[a], Huajun Zhao[a], Meimei Wang[b], Yongyang Zhu[c], Bo Li[a], Xueqing Yu[a], Jincheng Xu[a], Yajun Cheng[b], Liuzhang Ouyang[c, *], and Huaiyu Shao[a, *]

a. Joint Key Laboratory of the Ministry of Education, Institute of Applied Physics and Materials Engineering (IAPME), University of Macau, Macau SAR, China

b. Ningbo Institute of Materials Technology & Engineering, Chinese Academy of Sciences, 1219 Zhongguan West Road, Ningbo, 315201, Zhejiang Province, China

c. School of Materials Science and Engineering, Guangdong Provincial Key Laboratory of Advanced Energy Storage Materials, South China University of Technology, Guangzhou, 510641, China

Corresponding Author

*E-mail: meouyang@scut.edu.cn

*E-mail: hshao@um.edu.mo

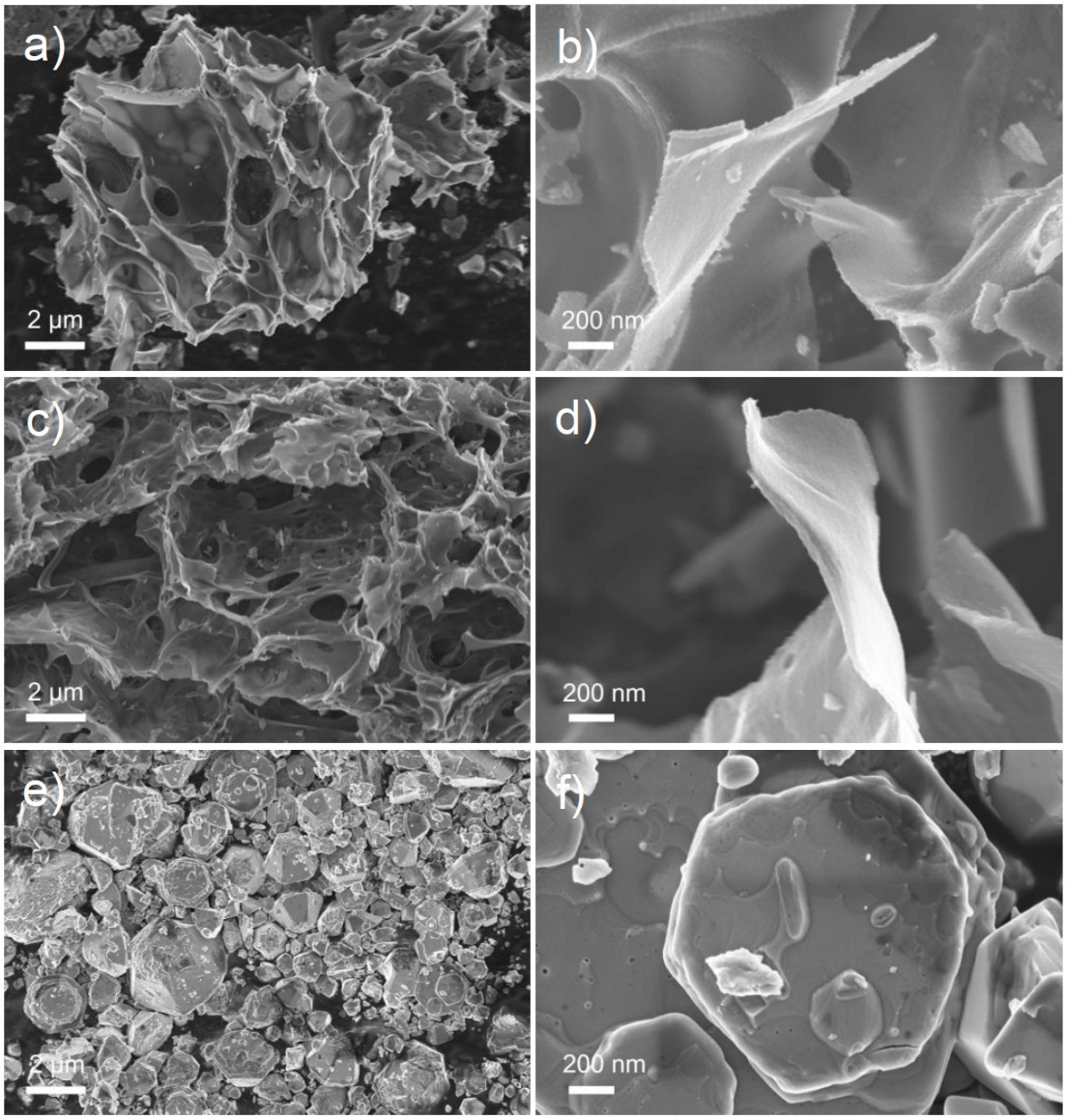

Fig. S1. SEM images of ZnO-NCNF-600 (a, b), ZnO-NCNF-800 (c, d) and pure ZnO (e, f).

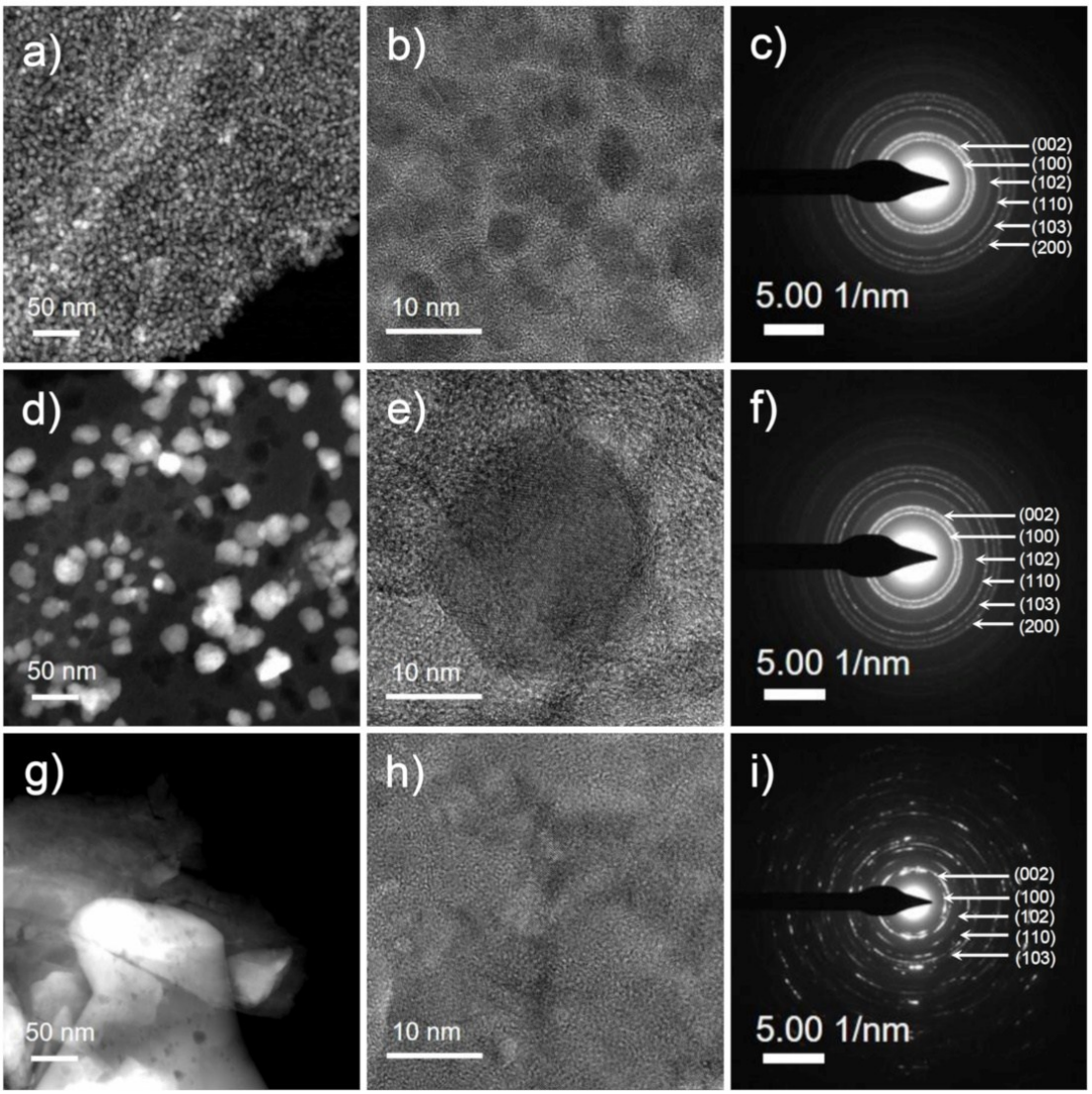

Fig. S2. HADDF STEM images, HRTEM images and selected area electron diffraction of ZnO-NCNF-600 (a-c), ZnO-NCNF-800 (d-f) and ZnO (g-i), respectively.

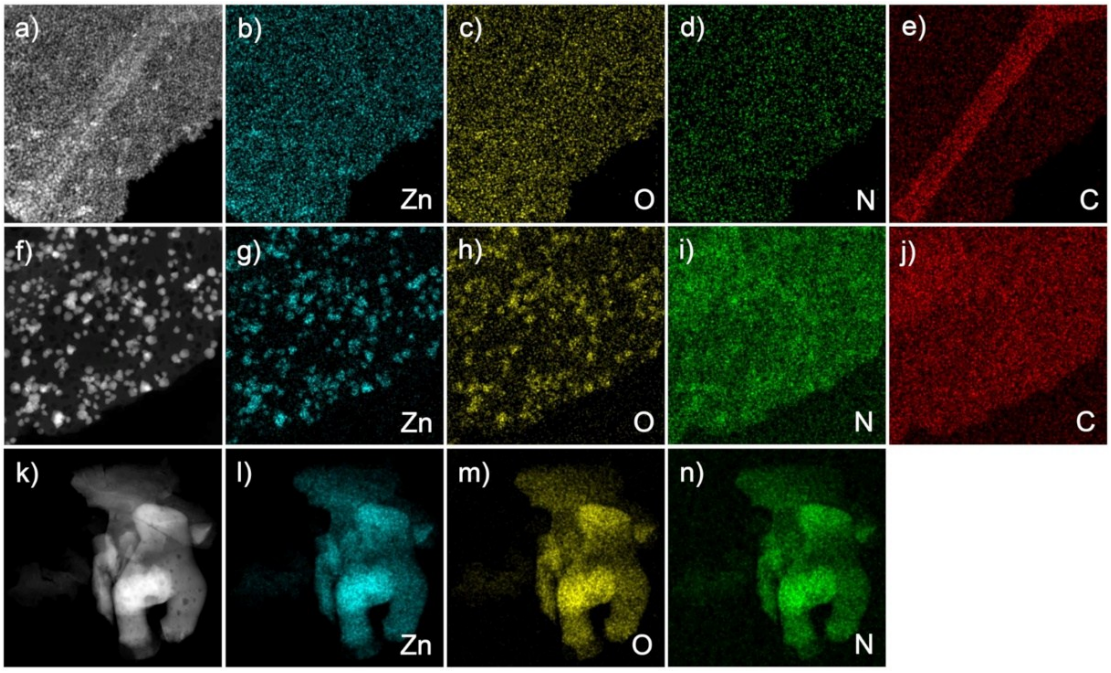

Fig. S3. HADDF STEM images and corresponding element mappings of ZnO-NCNF-600 (a-e), ZnO-NCNF-800 (f-j) and ZnO (k-n).

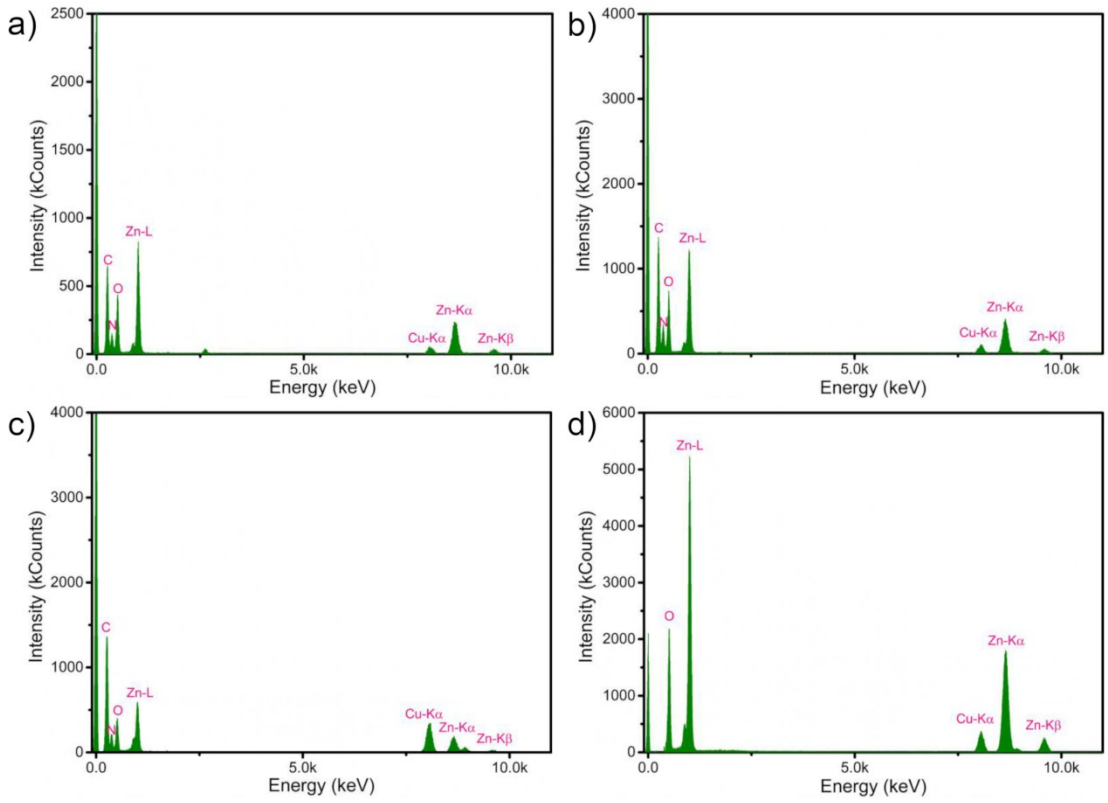

Fig. S4. EDS spectra of ZnO-NCNF-600 (a), ZnO-NCNF-700 (b), ZnO-NCNF-800 (c) and pure ZnO (d).

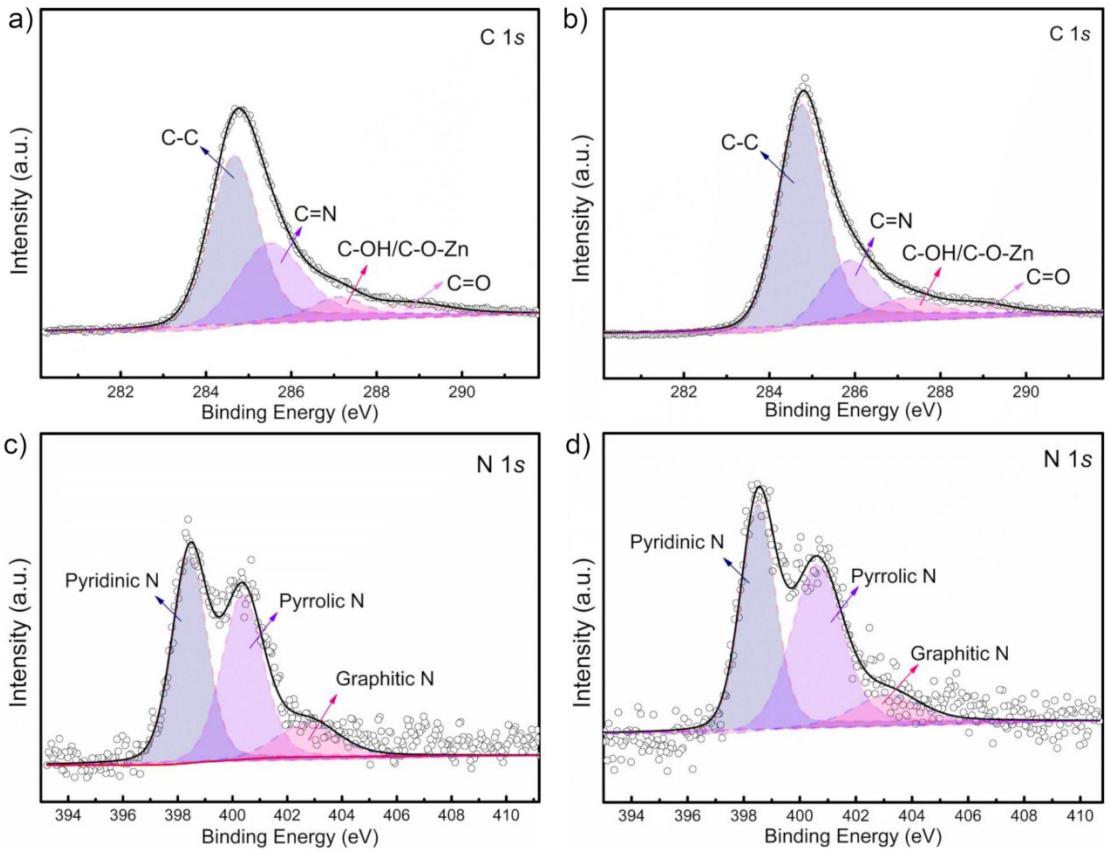

Fig. S5. The deconvoluted C1*s* (a) and N 1*s* (c) peaks for ZnO-NCNF-600 as well as the C1*s* (b) and N 1*s* (d) peaks for ZnO-NCNF-800 composite, respectively.

Table S1. Zn 2*p*, O1*s* binding energy and chemical composition of ZnO-NCNF composite and ZnO determined from the XPS results.

Sample	Zn 2*p*1/2 (eV)	Zn 2*p*3/2 (eV)	O 1*s* Peak one	O 1*s* Peak two	C (at.%)	N (at.%)	O (at.%)	Zn (at.%)
ZnO	1044.0	1020.8	529.8	531.3	-	2.94	33.78	25.67
ZnO-NCNF-600	1044.7	1021.5	530.6	532.4	64.51	7.65	20.55	7.29
ZnO-NCNF-700	1044.8	1021.7	530.7	532.5	61.42	7.33	26.06	5.19
ZnO-NCNF-800	1044.9	1021.8	530.8	532.7	74.73	7.24	14.36	3.67

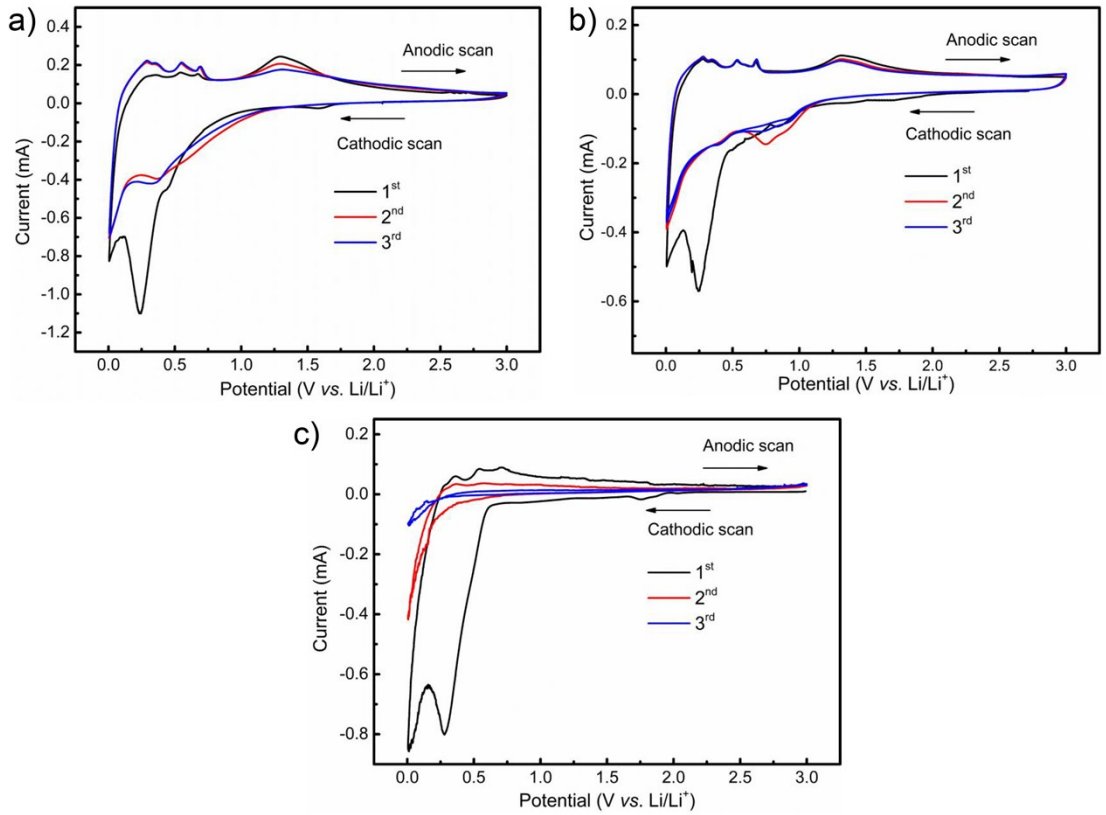

Fig. S6. Cyclic voltammetry curves of ZnO-NCNF-600 (a), ZnO-NCNF-800 (b) and pure ZnO (c) for the initial three cycles at the scan rate of 0.1 mV s^{-1}.

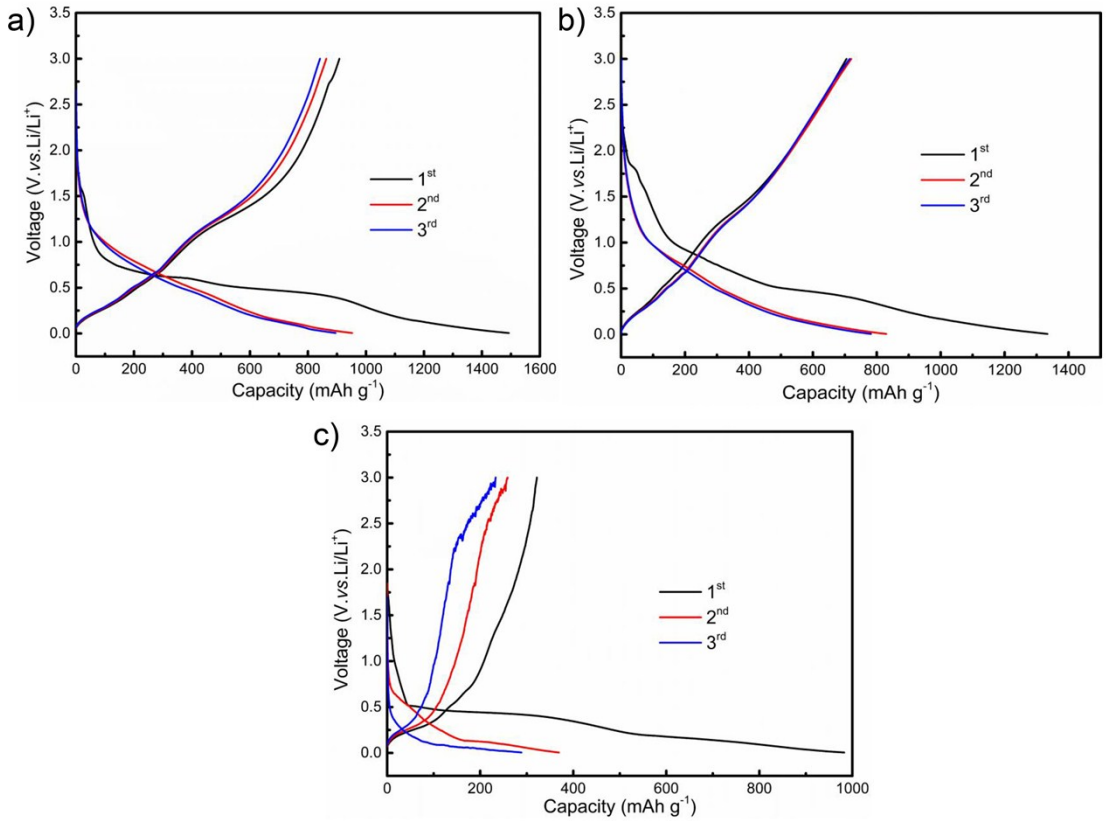

Fig. S7. Charge-discharge curves of ZnO-NCNF-600 (a), ZnO-NCNF-800 (b) and pure ZnO (c) electrode materials for the initial three cycles.

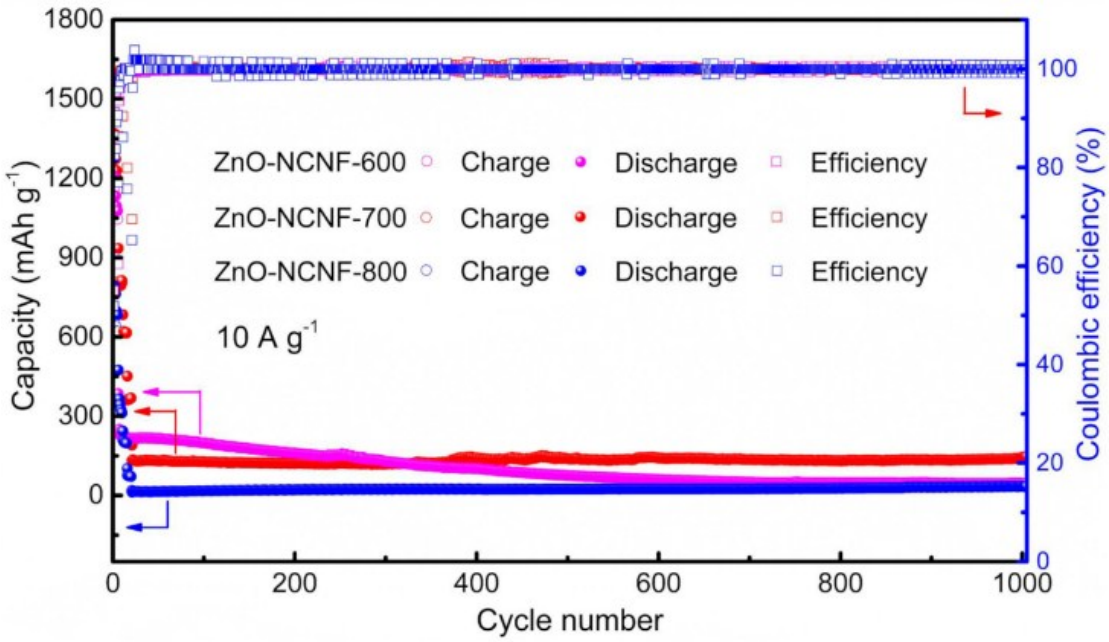

Fig. S8. Cyclic performance of ZnO-NCNF-600, ZnO-NCNF-700 and ZnO-NCNF-800 composites at a current density of 10000 mA g^{-1} for 1000 cycles.

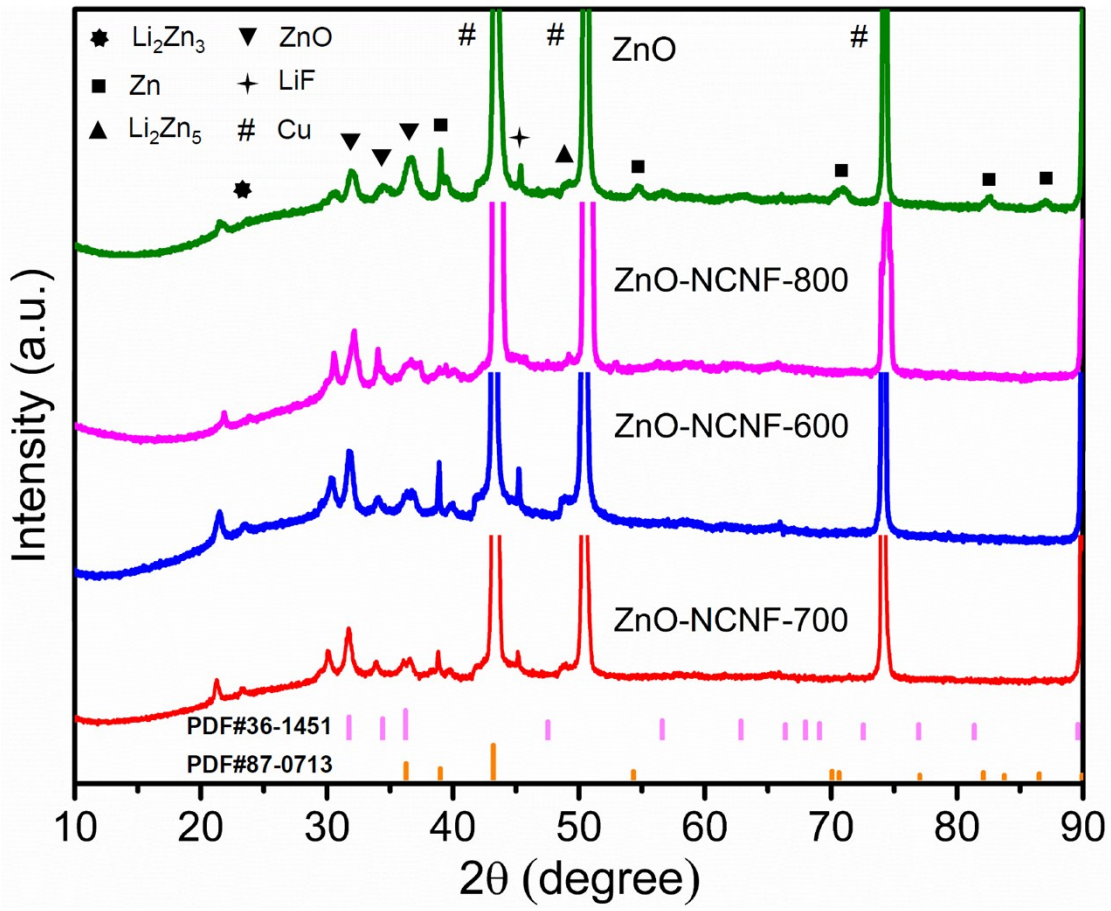

Fig. S9. XRD patterns of ZnO-NCNF-600, ZnO-NCNF-700, ZnO-NCNF-800 composites and pure ZnO after 750 cycles at 1000 mA g^{-1}.

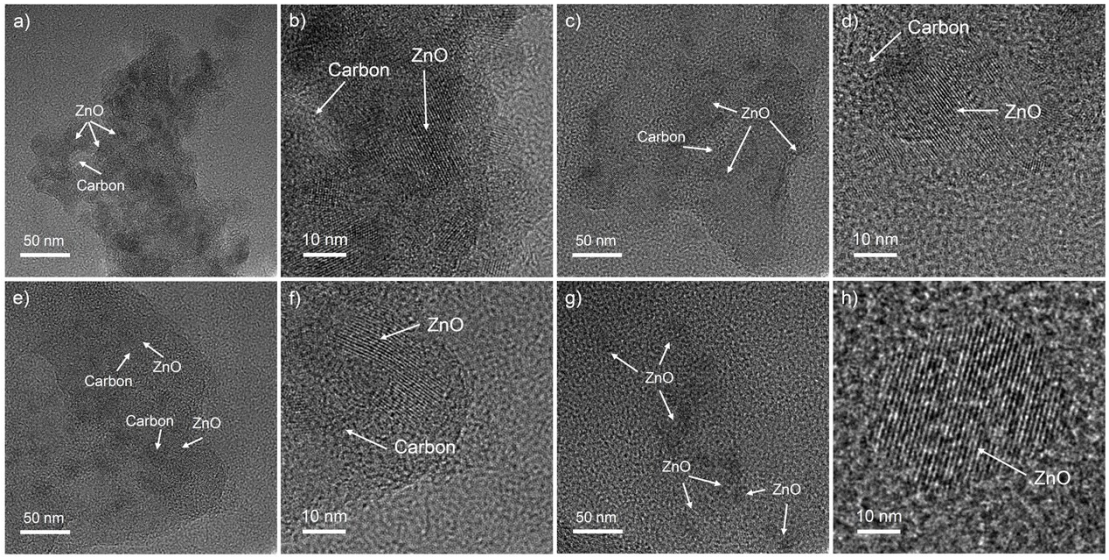

Fig. S10. TEM images of ZnO-NCNF-600 (a-b), ZnO-NCNF-700 (c-d), ZnO-NCNF-800 (e-f) composites and pure ZnO (g-h) electrode materials after 750 cycles at 1000 mA g^{-1}.

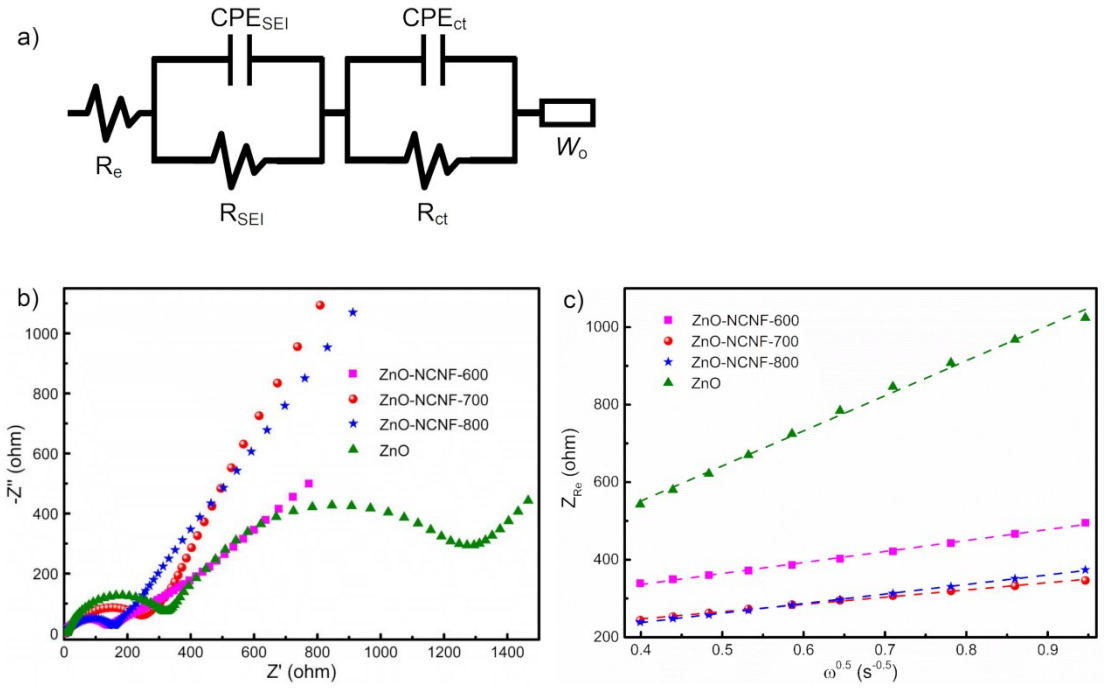

Fig. S11. (a) Equivalent circuit used to fit the impedance spectra and electrochemical impedance spectra of ZnO-NCNF-600, ZnO-NCNF-700, ZnO-NCNF-800 composites and pure ZnO after the first charge-discharge cycle (b). The relationship between the real resistance and the lower frequencies (c).

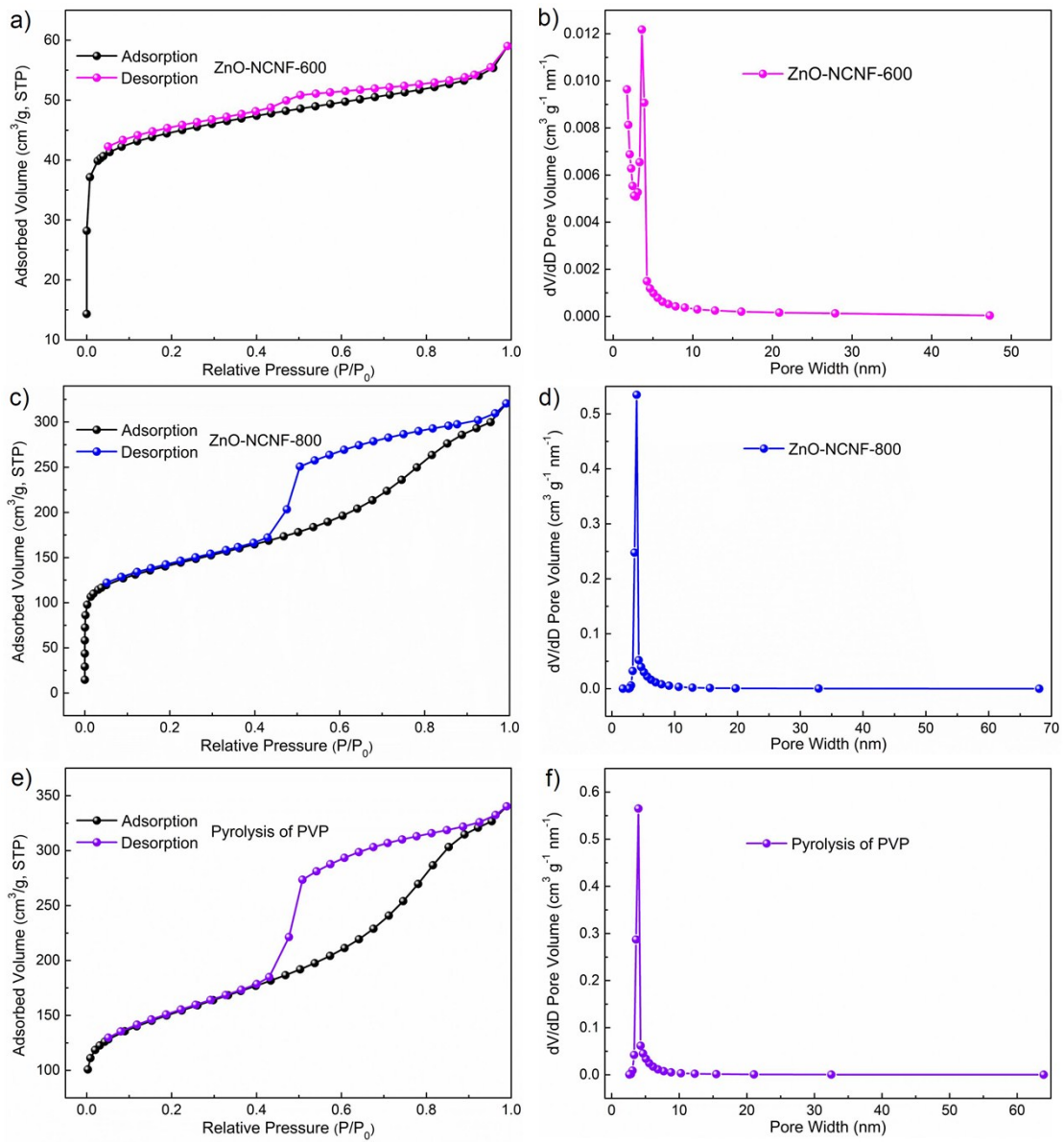

Fig. S12. Nitrogen adsorption-desorption isotherms and pore size distributions for ZnO-NCNF-600 (a-b), ZnO-NCNF-800 (c-d) and the pyrolysis of PVP (e-f).

The nitrogen adsorption-desorption isotherms and the pore size curves of ZnO-NCNF-600, ZnO-NCNF-800 and the annealed PVP are showed in **Fig. S12**. When compared with the ZnO-NCNF-600 (139.4 m^2 g^{-1}), the lower specific surface area of ZnO-NCNF-700 (129.8 m^2 g^{-1}) may be due to the decrease of carbon species. At this temperature, the obtained carbonaceous material deoxidizes ZnO and later evaporates forming mainly CO_2 and CO, thus reducing the carbon content. In addition, the much higher specific area of ZnO-NCNF-800 (467.1 m^2 g^{-1}) could be attributed to the vaporization of zinc oxide, leading to amounts of mesoporous in the composite (**Fig. S12**d).

Table S2. Comparison of lithium storage capabilities of ZnO-based anodes reported recently.

Materials	Current density (mA g^{-1})	Cycle number	Capacity (mAh g^{-1})	Reference
ZnO-NCNF	500	1000	770	This work
	1000	750	572	
	10000	1000	148	
Carbon/ZnO nanorod array	740	30	360	[1]
ZnO-loaded/porous carbon composites	100	100	653.7	[2]
ZnO encapsulated in 3D carbon framework	100	200	850	[3]
ZnO–CB nanocomposite	100	500	769	[4]
ZnO-NMPCS	200	100	1059	[5]
	5000	1800	425	
Carbon-coated ZNTs	100	100	410	[6]
ZnO/carbon CNF	100	100	818	[7]
ZnO@ZnO QDs/C NR Arrays	500	100	699	[8]
Three-dimensional carbon/ZnO	2000	700	260	[9]
Peapod-like ZnO@C	200	200	565	[10]
ZnO/3DOM-mC	97.8	100	973.3	[11]
Graphite coated-ZnO	1000	100	600	[12]
ZnO/C hierarchical porous nanorods	978	1500	623.94	[13]
ZnO@OMIL	500	100	620	[14]
	1000	1400	420	
Amorphous ZnO QDs/MPCBs	1000	400	510	[15]
ZnO QD/Graphene	1000	100	400	[16]
ZnO-QDs@CMS	1000	350	565	[17]
ZnO-VAGNs	350	250	450	[18]
ZnO/Cu/CNFs	500	50	618	[19]
	1000	50	493	

Table S3. The impedance results of the ZnO and ZnO-NCNF-700 electrode materials at various cycles.

ZnO	R_{SEI} (Ω)	R_{ct} (Ω)	σ_ω (Ω cm^2 s$^{-1/2}$)	D_{Li+} (cm^2 s^{-1})	ZnO-NCNF-700	R_{SEI} (Ω)	R_{ct} (Ω)	σ_ω (Ω cm^2 s$^{-1/2}$)	D_{Li+} (cm^2 s^{-1})
1st	324.5	780.5	904.6	2.9×10^{-14}	1st	131.6	127.7	187.0	6.8×10^{-13}
5th	348.9	1838	1294.4	1.4×10^{-14}	5th	138.8	198.6	214.6	5.2×10^{-13}
50th	331.8	1273	1473.5	1.1×10^{-14}	50th	129.0	232.4	197.7	6.1×10^{-13}
200th	401.2	6022	2157.6	5.0×10^{-15}	200th	88.1	67.6	74.7	4.3×10^{-12}
500th	572.9	16220	3404.8	2.1×10^{-15}	500th	78.2	61.4	58.4	7.1×10^{-12}

Table S4. Comparison of discharge capacity retention for full cell in this work with other reported previously.

Battery systems	Coulombic efficiency (%)	Discharge retention (%)	Reference
ZnO-NCNF~ $LiNi_{0.8}Co_{0.1}Mn_{0.1}O_2$	55.6% at 100 mA g^{-1}	99% at 60th cycle	This work
$NiCr_2O_4$/NG~$LiFePO_4$	-	37.2% at the 50$_{th}$ cycle	20
$Zn_3V_2O_8$~$LiFePO_4$	With prelithiation	80% at the 100th cycle	21
PEDOT-PSS/ZnO/C~ $LiNi_{0.6}Co_{0.2}Mn_{0.2}O_2$	With prelithiation	~66.4% at the 30th cycle	13
$ZnFe_2O_4$/G~$LiFePO_4$/C	~40.3% at 100 mA g^{-1}	~55.9% at the 10th cycle	22
ZnO@OMIL~$LiFePO_4$	85.4% at 1C rate	87.5% at the 100th cycle	14
α-Fe_2O_3~$LiFePO_4$	~68.5% at 1/20 C rate	~75% at the 30th cycle	23
CuO@MnO_2~$LiCoO_2$	~65% at 150 mA g^{-1}	~81.4% at the 100th cycle	24

References

1 J. Liu, Y. Li, R. Ding, J. Jiang, Y. Hu, X. Ji, Q. Chi, Z. Zhu and X. Huang, *J. Phys. Chem. C*, 2009, **113**, 5336-5339.

2 X. Shen, D. Mu, S. Chen, B. Wu and F. Wu, *ACS Appl. Mater. Interfaces*, 2013, **5**, 3118-3125.

3 C. Xiao, S. Zhang, S. Wang, Y. Xing, R. Lin, X. Wei and W. Wang, *Electrochim. Acta*, 2016, **189**, 245-251.

4 S. Lu, H. Wang, J. Zhou, X. Wu and W. Qin, *Nanoscale*, 2017, **9**, 1184-1192.

5 F. Sun, J. Gao, H. Wu, X. Liu, L. Wang, X. Pi and Y. Lu, *Carbon*, 2017, **113**, 46-54.

6 H.-S. Kim, H. Seo, K. Kim, J. Lee and J.-H. Kim, *Ceram. Int.*, 2018, **44**, 18222-18226.

7 E. Samuel, B. Joshi, M.-W. Kim, Y.-I. Kim, S. Park, T.-G. Kim, M. T. Swihart, W. Y. Yoon and S. S. Yoon, *J. Power Sources*, 2018, **395**, 349-357.

8 G. Zhang, S. Hou, H. Zhang, W. Zeng, F. Yan, C. C. Li and H. Duan, *Adv. Mater.*, 2015, **27**, 2400-2405.

9 Y. Zhao, G. Huang, Y. Li, R. Edy, P. Gao, H. Tang, Z. Bao and Y. Mei, *J. Mater. Chem. A*, 2018, **6**, 7227-7235.

10 Y. Hao, S. Wang, J. Zeng, H. Li, P. Yang, B. Liu, S. Zhang and Y. Xing, *Ceram. Int.*, 2018, **44**, 1321-1327.

11 F. Yin, Z. Zhang, Y. Zhang, C. Zhang and L. Xu, *Electrochim. Acta*, 2018, **270**, 274-283.

12 E. Quartarone, V. Dall'Asta, A. Resmini, C. Tealdi, I. G. Tredici, U. A. Tamburini and P. Mustarelli, *J. Power Sources*, 2016, **320**, 314-321.

13 G.-L. Xu, Y. Li, T. Ma, Y. Ren, H.-H. Wang, L. Wang, J. Wen, D. Miller, K. Amine and Z. Chen, *Nano Energy*, 2015, **18**, 253-264.

14 H. Song, J. Su and C. Wang, *Adv. Energy Mater.*, 2019, **9**, 1900426.

15 Z. Tu, G. Yang, H. Song and C. Wang, *ACS Appl. Mater. Interfaces*, 2017, **9**, 439-446.

16 X. Sun, C. Zhou, M. Xie, H. Sun, T. Hu, F. Lu, S. M. Scott, S. M. George and J. Lian, *J. Mater. Chem. A*, 2014, **2**, 7319-7326.

17 J. F. S. Fernando, C. Zhang, Konstantin L. Firestein, J. Y. Nerkar and D. V. Golberg, *J. Mater. Chem. A*, 2019, **7**, 8460-8471.

18 N. Li, S. X. Jin, Q. Y. Liao and C. X. Wang, *ACS Appl. Mater. Interfaces*, 2014, **6**, 20590-20596.

19 X. Shen, D. Mu, S. Chen, R. Huang and F. Wu, *J. Mater. Chem. A*, 2014, **2**, 4309-4315.

20 J. Tang, S. Ni, Q. Chen, X. Yang and L. Zhang, *J. Alloys Compd.*, 2017, **698**, 121-127.

21 Z. Yin, J. Qin, W. Wang and M. Cao, *Nano Energy*, 2017, **31**, 367-376.

22 A. Varzi, D. Bresser, J. von Zamory, F. Muller and S. Passerini, *Adv. Energy Mater.*, 2014, **4**, 1400054.

23 P. S. Veluri, A. Shaligram and S. Mitra, *J. Power Sources*, 2015, **293**, 213-220.

24 Q. Chen, B. Heng, H. Wang, D. Sun, B. Wang, M. Sun, S. Guan, R. Fu and Y. Tang, *J. Alloys Compd.*, 2015, **641**, 80-86.